SBIR/STTR RIGHTS NOTICE

These SBIR/STTR data are furnished with SBIR/STTR rights under Grant No. **DE-FG02-06ER84629.** For a period of 4 years after acceptance of all items to be delivered under this grant, the government agrees to use these data for Government purposes only, and they shall not be discussed outside the Government (including disclosure for procurement purposes) during such period without the permission of the grantee, except that, subject to the forgoing use and disclosure prohibitions, such data may be disclosed for use by support contractors. After the aforesaid 4-year period the Government has a royalty-free license to use, and to authorize others to use on its behalf, these data for Government purpose, but is relived of all disclosure prohibitions and assumes no liability for unauthorized use of these data by third parties. This notice shall be affixed to any reproductions of these data in whole or in part.

A New Class of Functionally Graded Ceramic-Metal Composites for Next Generation Very High Temperature Reactors

FINAL REPORT

Contract No: DE-FG02-06ER84629
Contract Period: 7/01/06-3/31/07
NEI Project Code: NEI43049

NEI Corporation
400E Apgar Drive
Somerset, NJ 08873
Ph: (732) 868-3141
www.neicorporation.com

Principal Investigator: Dr. Mohit Jain
Dr. Ganesh Skandan
Dr. Gordon E. Khose, & Mrs. Judith Maro, Nuclear Reactor Laboratory, MIT

A. INTRODUCTION

Generation IV fission reactor systems, such as high temperature gas reactors, molten salt reactors and vapor core reactors, operate at temperatures > 900 ^{o}C. The components operating at these temperatures require excellent thermo-mechanical properties, i.e. exceptional high temperature strength, good high temperature creep strength, high thermal conductivity, low thermal expansion coefficient, and good fracture toughness.

Tungsten and molybdenum based alloys show sufficient creep strength at high temperatures, but are inherently brittle. Although it has been observed that a fine grain size suppresses propagation of cracks in high atomic mass refractory metals, hence improving toughness,[1] the properties degrade with irradiation and upon exposure to oxygen. Ceramic materials (e.g., HfB_2, ZrC, SiC, and SiC/SiC fiber composites) have shown promise for use at high temperature. However, in the case of composites, the fiber-matrix interface degrades with irradiation and environmental exposure, leading to debonding. In addition, with increasing neutron exposure, differential swelling between the fiber and the matrix gives rise to internal stresses. This results in cracking at the fiber-matrix interface[2]. Stand-alone HfB_2, ZrC, and SiC components lack the toughness of fine-grained refractory metal alloys.

In the Phase I program, we began developing a **"functionally graded"** material, which combines the beneficial properties of both tungsten heavy alloys (*hereafter* W-Ni-Fe) and SiC. In a functionally graded material, the concentrations of the dissimilar phases (i.e., metal and ceramic in this case) vary gradually through the section of the material. This leads to structural advantages, as outlined below in section B.

Figure 1 shows a schematic of the W-Ni-Fe - SiC functionally graded material fabricated during the Phase I program. The top surface has the highest concentration of SiC, while the bottom surface is free of SiC. Figure 2 shows a photograph and SEM micrographs of the material, confirming the functionally graded microstructure. A variation of this structure, which was also fabricated in the Phase I program, is a core that is free of SiC, while all the outer surfaces have the highest concentration of SiC. To the best of our knowledge, such functionally graded metal-ceramic composites have not been explored to date for use in nuclear reactors. Neutron irradiation experiments conducted at the MIT Nuclear Reactor Facility on these samples, albeit very preliminary due to the time constraints of the Phase I program, showed that there is no delamination or structural degradation.

[1] Kurishita, H. and Yoshinaga, H., Materials Forum, v13, 1989, p161

[2] Allen, T., Brummer, S., Kassner, M., Odette, R., Stoller, R., Was, G., Wolfer, W., Zinkle, S., Elmer, J., and Motta, A., "Higher temperature reactor materials workshop, March 18-21, 2002", La Jolla, CA. (http://www.doe.gov/bridge)

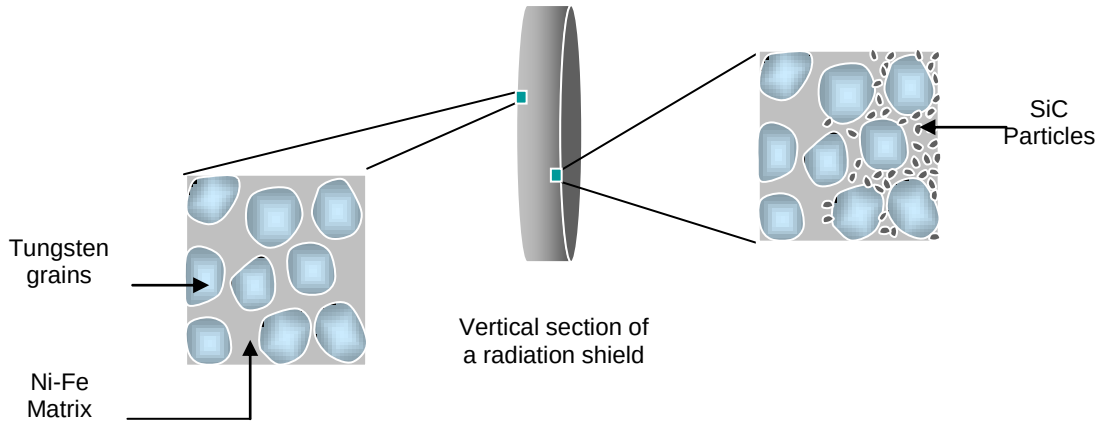

Figure 1: Schematic of the functionally graded material fabricated during Phase I program.

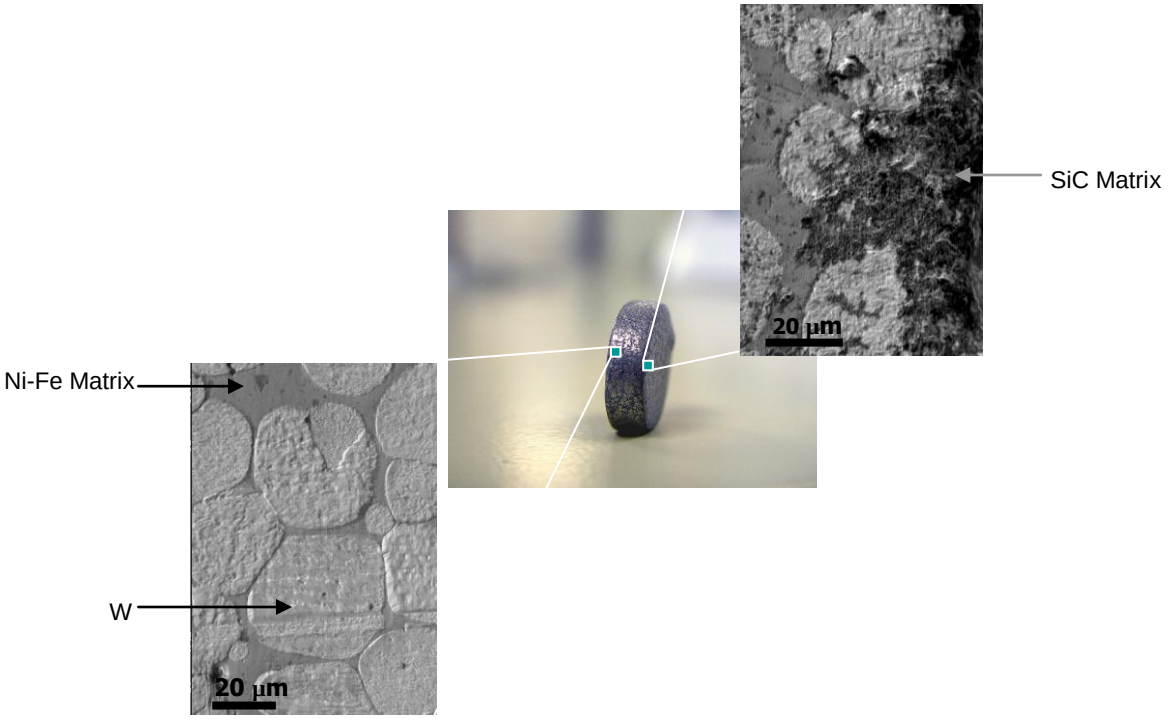

Figure 2: Photograph and scanning electron micrograph (SEM) of functionally graded W-Ni-Fe-SiC composite.

The following were the additional accomplishments of the Phase I program, leading us into the next phase of product development:

- Demonstrated that graded porosity can be introduced in a partially sintered W-Ni-Fe substrate. Figure 3 shows SEM micrographs of the samples, before and after the introduction of porosity gradient.

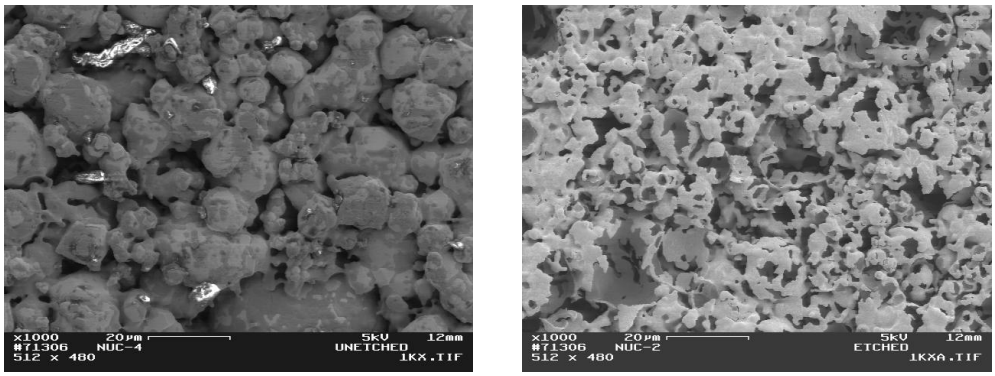

(a) **(b)**

Figure 3: (a) Partially sintered W-Ni-Fe sample; and **(b)** sample after porosity gradient generation.

- Demonstrated that SiC nanoparticles can be deposited in the pores and surface of porosity graded samples, by using an electrophoretic deposition method.
- Demonstrated that the samples can be sintered to full density by liquid phase sintering, while retaining the desired structure, Figure 2.
- Demonstrated that functionally graded samples do not degrade during initial neutron irradiation testing.

Following is the technical background, followed by a synopsis of the experimental work that was performed during the course of the Phase I program:

B. Technical Background

Effect of neutron irradiation on SiC

Snead et al[3] studied the effect of fission neutrons on SiC, by irradiating monolithic SiC and SiC composites in the temperature range of 90 – 1000 ^{o}C and dose range of 1.1 – 7.7 × 10^{25} n/m^2 (E>0.1 dpa). The monolithic SiC was fabricated by chemical vapor deposition process, while the composite was fabricated by chemical vapor infiltration of SiC in SiC-based fibers. Under the irradiation conditions that were used, they did not observe any change in the strength and variability of strength for both monolithic SiC and SiC composites. However, they pointed out that in the case of monolithic SiC, the effect of irradiation on the mechanical properties is dependent on the stoichiometry of the SiC, which depends on the process by which they are synthesized. For example, in the case of reaction bonded SiC, carbon and molten silicon are added to SiC, which results in the presence of 8-10 wt% unreacted silicon, which segregates at the grain boundary. Similarly, sintering aids such as aluminum and boron used in the synthesis of SiC often segregate at the grain boundaries. These impurities enhance the degradation of monolithic SiC at high temperatures and in the presence of irradiation. Figure 4 shows that at doses below 10 dpa, no degradation in the strength of CVD SiC was observed. However, in all cases there was a reduction in the Weibull modulus.

[3] Snead, L. L., Hinoki, T., and Katoh, Y., "Strength of neutron irradiated silicon carbide and silicon carbide composite", Fusion Materials Volume 33, Semiannual Progress Report for Period Ending December 31, 2002, page 49-57, (https://www.ms.ornl.gov/programs/fusionmatls/pubs/dec2002index.htm, accessed on 4/3/07).

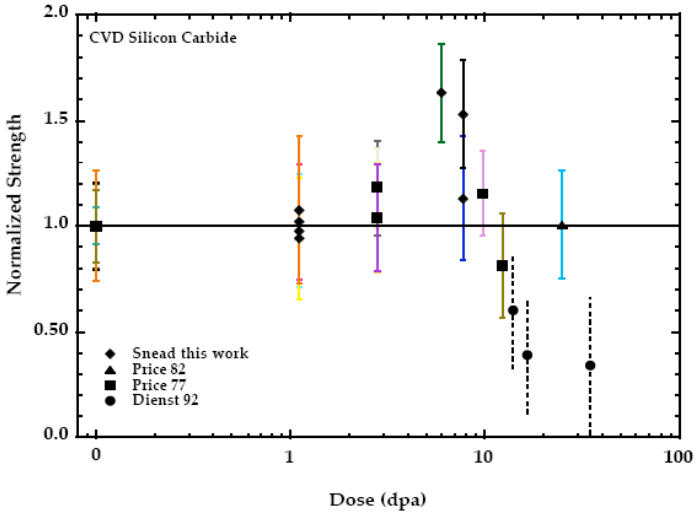

Figure 4: The variation in the normalized strength of CVD SiC with the amount of irradiation (taken from Snead et al 2002, Ref. 3).

In order to illustrate that the process used to produce SiC has an effect on the irradiation properties of SiC, Snead et al compiled data from various researchers, who used powder processed monolithic SiC. As can be seen from Figure 5, the normalized strength degrades significantly, even at low doses. According to them, this is due to the presence of impurities in SiC. For example, presence of free silicon in the case of Norton NC-430 leads to different amounts of swelling between SiC and silicon. In the case of boron doped SiC, where boron was added as a sintering aid, the (n, α) reaction takes place, which leads to formation of He bubbles.

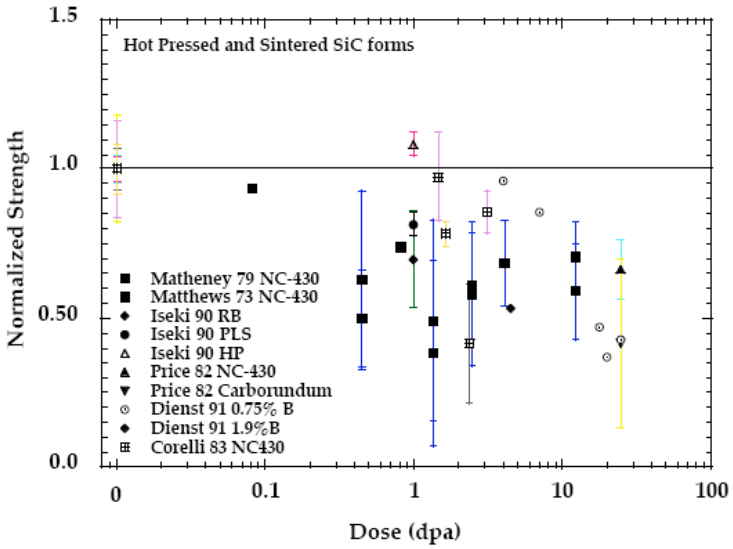

Figure 5: Variation in strength of powder processed monolithic SiC, with irradiation dose (taken from Snead 2002, Ref. 3).

Okamura et al[4] studied the effect of neutron irradiation on the structure and strength of SiC fibers. Two types of SiC fibers were used. One was an amorphous SiC fiber, and the other was a microcrystalline fiber. They observed that the density and tensile strength of both the fibers gradually increased with the amount of neutron fluence. The increase in the density was attributed to the increase in the close packing of the atoms. They observed no change in the atomic arrangement in the amorphous SiC fibers. In contrast, in the case of microcrystalline SiC fibers, disorder was induced due to neutron irradiation, when the irradiation was performed at 423 K. However, when the irradiation was performed at 923 K, the atomic arrangement in amorphous fiber became ordered, while the atomic arrangement of the microcrystalline SiC was not changed. They also observed that the density, tensile strength and the Young's modulus of amorphous and microcrystalline SiC fibers were the same after neutron irradiation of 2×10^{24} n/m^2 at 423 K, and 9×10^{24} n/m^2 at 923 K.

Nogami et al [5] studied the effect of He pre-implantation and neutron irradiation on the mechanical properties of SiC/SiC composites. They observed that the ultimate fracture strength, the elastic modulus and the proportional limit stress decreased due to neutron irradiation by about 50%, 10% and 55%, respectively. However, when they studied the irradiation behavior of the elastic modulus of the SiC matrix and the fiber individually, it was found that there was no change in the elastic modulus of the matrix, and the modulus of the fiber actually increased by ~ 30%. Thus, the rule of mixtures used in composites does not seem to be applicable for the neutron irradiated composite. Therefore, they postulated that degradation (e.g. cracking and debonding) of the interface between the SiC matrix and the fiber occurred due to neutron irradiation, hence deteriorating the properties of the composite. This was confirmed by Yamada et al[6], who showed the presence of microcracking and debonding of the C-interface in a Hi-Nicalon/C/SiC composite due to C-ions irradiation up to about 10 dpa at 800 ^{o}C.

The above discussion demonstrates that despite the promise of SiC, there are several technical issues with respect to both monolithic and fiber composites that need to be overcome to enable the use of SiC. For reasons explained below, the proposed approach of functionally graded metal-ceramic composites can overcome these limitations. In order to understand the behavior of these graded materials, a good place to start would be at relatively small dpa levels of irradiation, which is what we have started doing in Phase I.

Functionally graded materials and relation to the present work

Functionally graded materials (FGMs) were first proposed by Niino and Maeda[7] to overcome the issue of thermal stresses induced in an aerospace component, which was subjected to a high thermal gradient. Since then, various types of functionally graded materials have been fabricated. Traditionally, these materials are classified into three categories[8]: (i) interface FGM, (ii) surface FGM, and (iii) bulk FGM. In the case of interface FGMs, the composition at the interface of two dissimilar materials, which are supposed to be joined together, is varied in order

[4] Okamura, K., Matsuzawa, T., Sato, M., Kayano, H., Morozumi, S., Tezuka, H., and Kohyama, A., "Effects of neutron irradiation on fine structure and strength of SiC Fibers", J. Nuc. Mat., v155-175, 1988, p 329-333.

[5] Nogami, S., Hasegawa, A., Sned, L. L., Jones, R. H., and Abe, K., "Effect of He pre-implataion and neutron irradiation on mechanical properties of SiC/SiC composite", J. Nuclear Materials, v329-333, 2004, p577.

[6] Yamada, R., Nogami, S., Hasegawa, A., Abe, K., and Taguchi, T., J. Nuclear Materials, v283-287, 2000, p268.

[7] Niino, M. and Maeda, S., ISIJ, v30, 1990, p699.

[8] Rowlings, R. "Tailoring properties: functionally graded materials", Mater. World, v3, 1995, p474-475.

to reduce the thermal stresses. Thermal stresses are generated when these materials are joined together due to the difference in the thermal expansion coefficient of the constituents. Surface FGMs are fabricated when dissimilar properties are required on the surface and the interior of the component. For example, if a coating of a hard or corrosion resistant material is required on the surface, but the interior has to be ductile, then the traditional way is to coat the surface. During service, these traditional components can fail prematurely when the top coat fails at the interface, and the soft core is exposed. However, in the case of FGMs, the interface problem is eliminated as the composition varies gradually, hence it can lead to the increase in the life of the component. In the case of bulk FGMs, it is desired that the material at the surface of the component has one property, a different property over a significant depth from the surface, and a completely different property at the core. For example, one may desire high hardness on the surface, high stiffness just below the surface, and high fracture toughness, in the core.

Delfosse et al[9] had done significant study on the prediction and measurement of residual stresses generated in functionally graded materials. They fabricated three different FGM materials, namely Cu-Ni, CrNi-ZrO_2 and WC-Co. The stress profile for various composites was generated using the finite element method, namely numerical solutions obtained by ABAQUS code. Figure 6 shows the variation in the residual stresses in the case of CrNi-ZrO_2 composite, when three different composition profiles were used. As can be observed from the figure, the magnitude of induced residual stresses was maximum in the case where there was no gradient, and residual stresses are significantly reduced in the case of graded composites. A similar behavior was observed in the case of WC-Co graded composites , where the composition of WC and Co was gradually varied (Figure 7). It was also observed that the amount of residual stresses is dependent on the gradient profile, which itself is dependent on the composition and the thickness of the graded layer.

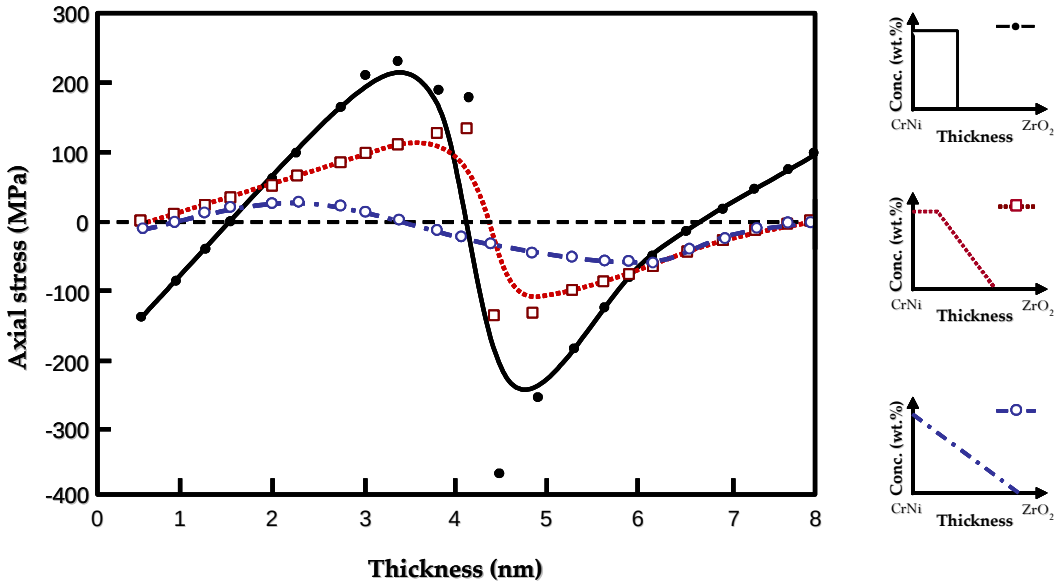

Figure 6: Simulated residual stress profile in the case of CrNi-ZrO_2 composite (adopted from Delfosse et al was redrawn for clarity).

[9]Delfosse, D., Cherradi, N., and IIschner, B, "Numerical and experimental determination of residual stresses in graded materials", Composites Part B (Engg.), v28B, n 1-2, 1997, p127-141.

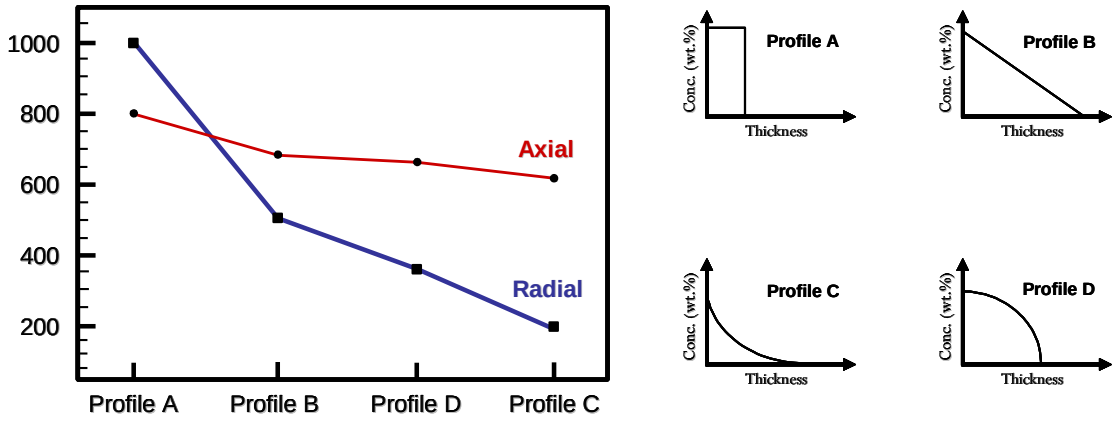

Figure 7: Simulated residual stress profiles in the case of WC-Co composites (graph from Delfosse et al was redrawn for clarity).

As can be observed from the above discussion, the fabrication of functionally graded materials leads to a reduction in residual stress, when two dissimilar materials are joined together. Nuclear irradiation and exposure to high temperature leads to stresses in materials, and so the use of a functionally graded composite should alleviate the problem of degradation of mechanical properties. In the present approach, the SiC on the surface will provide the irradiation resistance and minimize oxidation of the W-Ni-Fe, while W-Ni-Fe will provide the structural integrity, and toughness. Additionally, since there is a difference in the densities of the two components, SiC (~3.1 g/cc) and W-Ni-Fe (17.3 g/cc), the overall weight of the component will be reduced. This will also enable a reduction in the thickness of the components. Further, it is observed that the prolonged neutron irradiation of SiC leads to swelling[10] and increase in volume. This increase in volume will lead to significant increase in residual stresses in the composites, if the composite is not graded. Furthermore, the metal provides the integrity to the structure, when SiC is transformed from crystalline to amorphous state.

C. Objectives

The objectives of the Phase I program were:

(i) to demonstrate the feasibility of producing dense SiC-W composite samples with functionally graded interface;

(ii) to demonstrate that a sintered SiC-W functionally graded composite will have variation in the hardness with the variation in SiC ;

(iii) to demonstrate that the proposed SiC-W composite can withstand neutron irradiation.

We have accomplished the above mentioned objectives during the Phase I program and following are descriptions of Phase I experimental work.

[10] Henager, C. H., Le, E. A., and Jones, R. H., J. Nuc. Mat., v329-333, 2004, p502-506.

D. Descriptions of Phase I Experimental Work

D.1 Synthesis of W-Ni-Fe composite powders

The choice of composition was based upon what is currently being used for producing Tungsten Heavy Alloys (WHAs) for radiation shielding applications[11]: 90 wt% W, 8.8 wt% Ni, and 1.2 wt% Fe. Commercially available W powder with a particle size of ~20 μm was used in all the experiments. Ni-acetate and Fe-oxalate were used as the source of Ni and Fe, respectively. Initially, pure Ni-acetate and Fe-oxalate were heat treated separately at 500 ^{o}C in 70-80% H_2 and 20-30% N_2 atmosphere to confirm the formation of Ni and Fe metals. Figures 8 and 9 show X-ray diffraction patterns of the as-synthesized powders, which confirm the formation of the two metals upon reduction of the precursors. Subsequently, Ni-acetate and Fe-oxalate were dissolved in ethanol in a stoichiometric ratio, followed by addition of W powder. The powder was mixed in the solution using a high shear mixer. Finally, the powder was dried by evaporating the ethanol in a rotovapor and then heat treated at 500 ^{o}C for 2 hours in 70-80% H_2 and 20-30% N_2. Figure 10 shows the X-ray diffraction pattern of the as-synthesized composite powder, which demonstrates the formation of Ni and shows the presence of W as well. Fe was not detected due to the small amount in the powder.

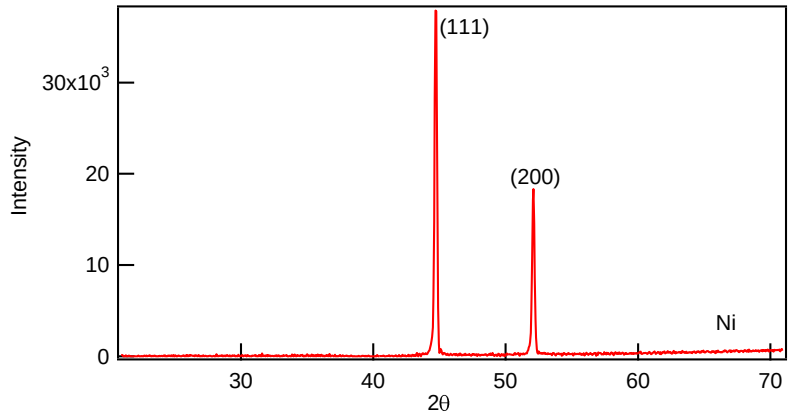

Figure 8: X-ray diffraction pattern of as synthesized Ni powder.

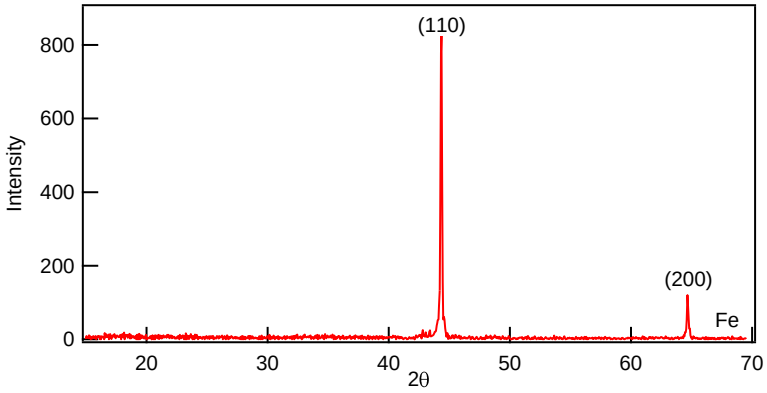

Figure 9: X-ray diffraction pattern of as synthesized Fe powder.

[11] www.atifirthsterling.com

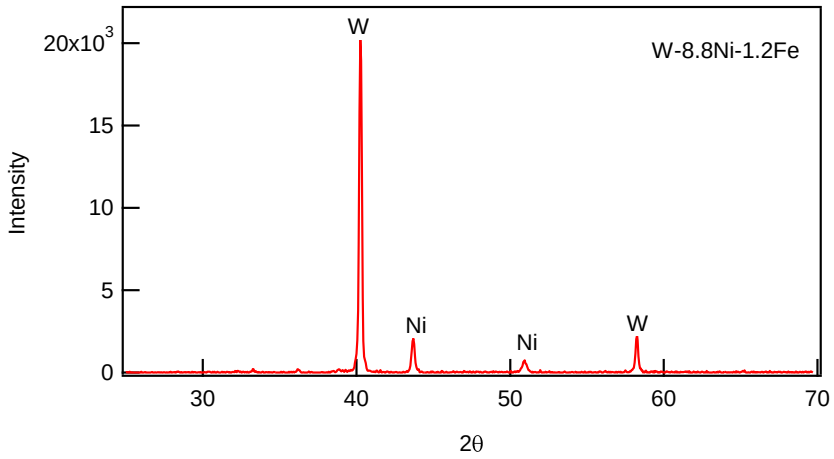

Figure 10: X-ray diffraction pattern of W-Ni-Fe composite powder.

D.2 Compaction of W-Ni-Fe composite powders

The as-synthesized W-Ni-Fe powder was mixed with poly (vinyl butyral), which acts as a binder. Our prior work has shown that 0.48wt% of binder is the optimum amount for maximizing the green density in the pellet. The binder was mixed in ethanol, which was followed by addition of powder. The powder was mixed with the binder using a magnetic stirrer. Subsequently, the powder was dried using a rotovapor. The dried powder was compacted using a Carver hydraulic press. Initially, a 1.6 cm diameter die was used to make the pellets. In the latter part of the program, we also used a 0.6 cm die, due to the requirement of smaller sized samples for irradiation tests. The compacts were heat-treated for binder burnout and partial sintering. This was achieved by initially heating the compacts to 700 ^{o}C for 2 hours in a H_2/N_2 gas mixture, followed by further heating the samples at 1000 ^{o}C for 1 hour. Table I shows the densities of the samples after partial sintering. These samples were used for electrochemical etching and SiC deposition experiments.

Table I: Densities of partially sintered W-Ni-Fe samples

Sample ID	Density (g/cc)	Relative Density[12] (%)
NUC-1	11.79442	68.4131
NUC-2	11.60525	67.31586
NUC-3	11.69765	67.85181
NUC-4	11.67547	67.72313
NUC-5	10.2171	59.26394
NUC-6	10.30692	59.78494
NUC-7	10.4328	60.51511
NUC-8	10.34593	60.0112
NUC-9	9.893358	57.38607
NUC-10	10.18694	59.089
NUC-11	10.14227	58.82986
NUC-12	10.14119	58.8236
NUC-13	10.03182	58.18919
NUC-14	8.66579	50.2656
NUC-15	8.838398	51.26681
NUC-16	8.820237	51.16147
NUC-17	8.005692	46.43673
NUC-18	8.251233	47.86098
NUC-22	8.721115	50.58651
NUC-23	9.158816	53.12538
NUC-24	8.905828	51.65794
NUC-25	8.800584	51.04747
NUC-26	8.608344	49.93239
NUC-27	8.600671	49.88788
NUC-28	10.62722	61.64279
NUC-29	10.40365	60.34603
NUC-30	10.83296	62.83617
NUC-31	10.56837	61.30143

D.3 Porosity Gradient Generation

Figure 11 shows SEM micrographs of samples before and after generation of porosity gradients, at various processing parameters. The clearly demonstrates the control in porosity gradient, that can be achieved by varying the processing parameters.

[12] Relative density refers to the density of the compact relative to a fully dense non-porous W-Ni-Fe sample. The density of a fully dense sample is calculated by taking the crystal densities of the three components and their weight fraction in the material

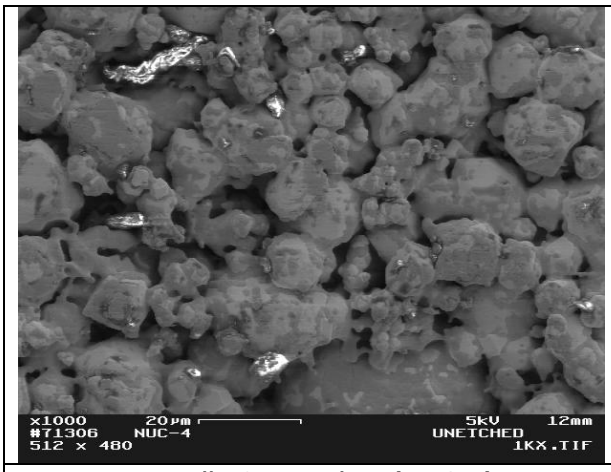

Partially Sintered W (NUC-4)

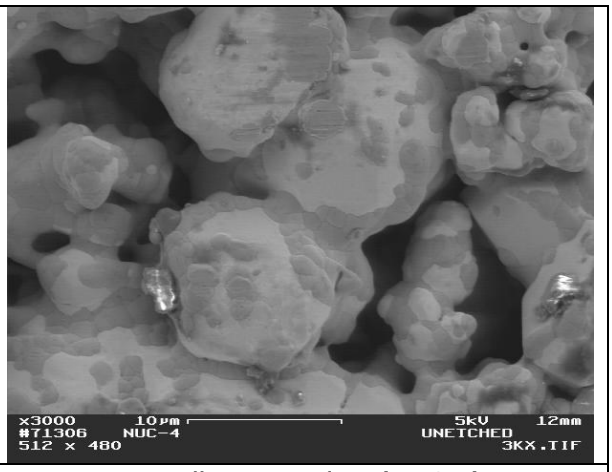

Partially sintered W (NUC-4)

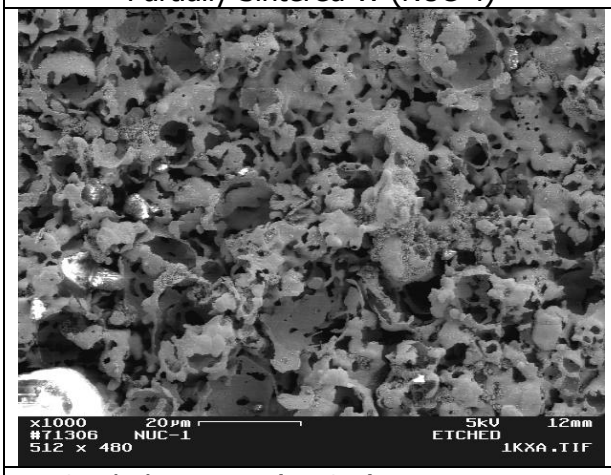

Graded porosity (NUC-1) , Parameter-1

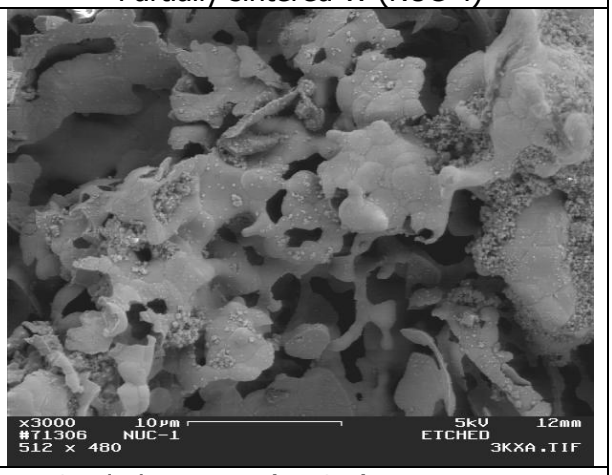

Graded porosity (NUC-1), Parameter-1

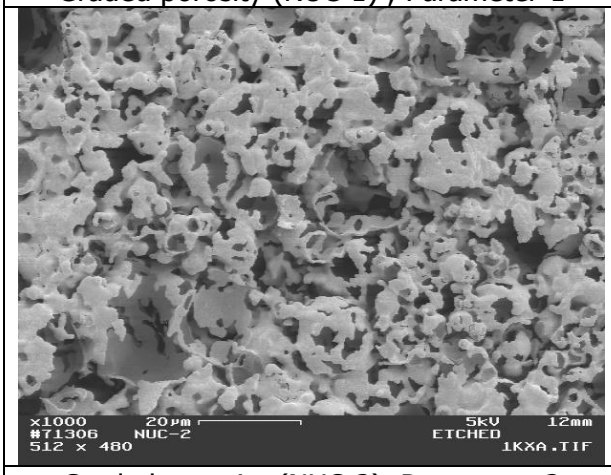

Graded porosity (NUC-2), Parameter-2

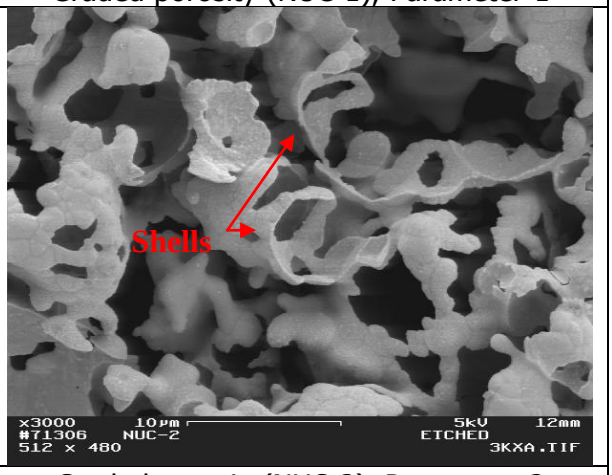

Graded porosity(NUC-2), Parameter-2

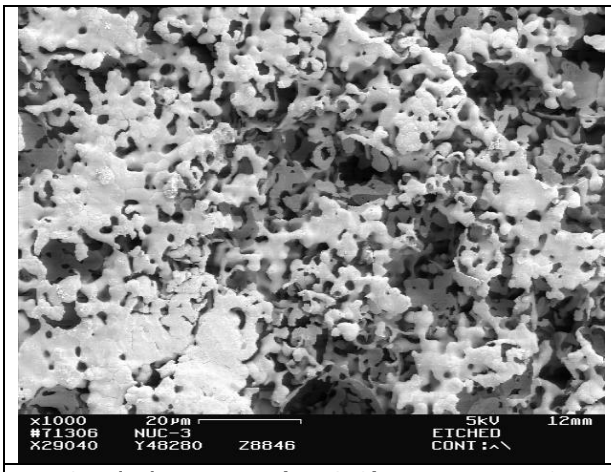

Graded porosity (NUC-3), Parameter-3

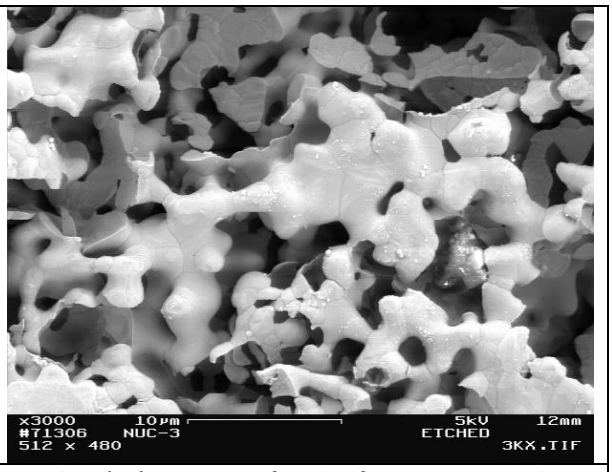

Graded porosity (NUC-3), Parameter-3

Figure 11: SEM micrographs of unetched and electrochemically etched W-Ni-Fe partially sintered samples.

D.4 Electrophoretic Deposition of SiC

Electrophoretic deposition of SiC on etched W-Ni-Fe samples was carried out using the setup shown below. This power supply has a capacity of 100 kV and 11 mA. Figure 12 shows a photograph of the setup. We used ethanol as the medium for dispersion. For the initial set of experiments, ~1 µm SiC powder was used, and later we switched to nanocrystalline SiC (*hereafter* nano-SiC) powder, in order to increase the amount of infiltration in the etched sample. Figure 14 shows the X-ray diffraction pattern and Figure 13 shows particle size distribution of nano-SiC used for electrophoretic deposition. Initially, a blank coupon was used to determine the charge on the surface of SiC particles. The particles were observed to deposit on the cathode (-ve charge), which means that the particles were positively charged. A voltage in the range of 100-160 V was applied in the constant current mode. Some of the smaller samples were coated on both sides to make them suitable for irradiation testing.

Figure 12: Electrophoretic deposition setup to deposit SiC.

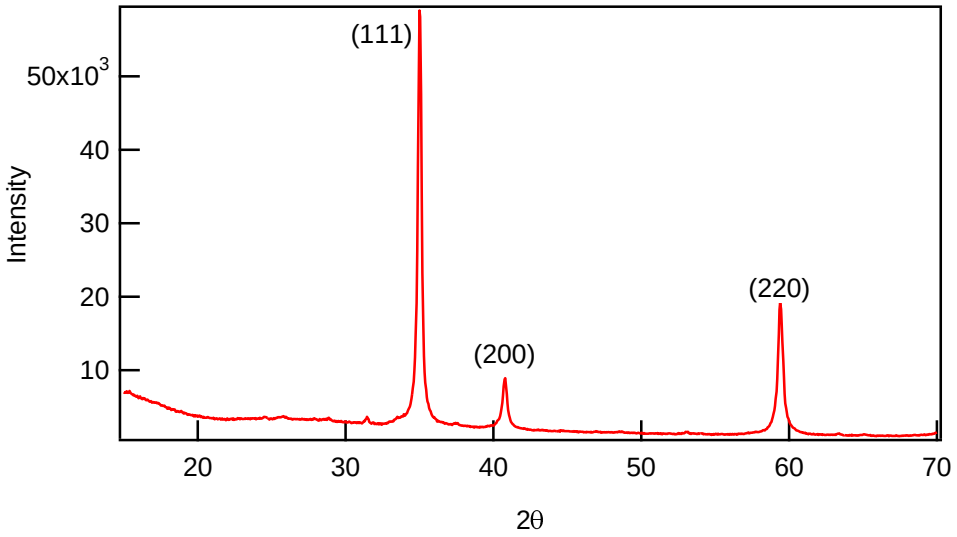

Figure 13: X-ray diffraction pattern of nano-SiC used for electrophoretic deposition.

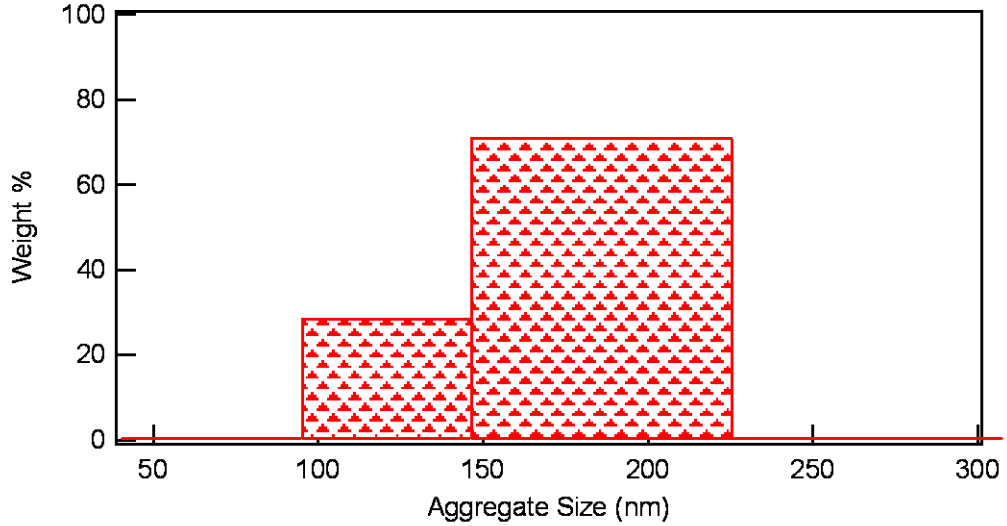

Figure 14: Aggregate size distribution of nano-SiC used for electrophoretic deposition.

D.5 Infiltration of polymer SiC precursor on samples after electrophoretic deposition

Some of the samples were infiltrated with a SiC precursor, Ceraset 20, after electrophoretic deposition of SiC. Ceraset 20 is a low viscosity polysilazane, which converts into SiC by heating at 1000 ^{o}C in an argon atmosphere. Figure 15 shows the structure of Ceraset 20[13]. Initially, the polymer was infiltrated by a vacuum infiltration method, to fill the pores left after electrophoretic deposition. Subsequently, the samples were heat treated in an argon atmosphere at 1000 ^{o}C to convert the polymer to SiC. Some of the samples were repeatedly coated with a mixture of nano-SiC / Cerasat-20 to increase the amount of SiC in the samples. These samples were again heat treated at 1000 ^{o}C for 1 hour, followed by final sintering at 1470 ^{o}C.

[13] http://www.kiondefense.com/bulletins/TB1.pdf

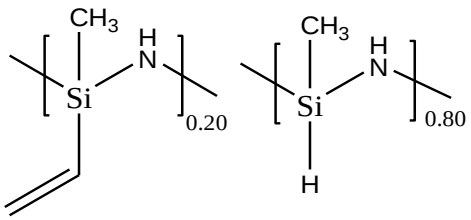

Figure 15: Molecular structure of Ceraset 20.

D.6 Sintering of samples and microstructure characterization

After electrophoretic deposition and polymer infiltration (in some cases as described above), the samples were sintered at 1470 ^{o}C for 1 hour in H_2 atmosphere. This temperature is slightly above the melting point of Ni (m.p. 1453 ^{o}C), thereby leading to liquid phase sintering. Some of the sintered samples were evaluated using an SEM. Several samples were also characterized for SiC content by measuring the final weight gain of the samples. Figure 16 shows photographs and SEM micrographs of NUC-28, fabricated by electrochemical etching, followed by infiltration of SiC by electrophoretic deposition and infiltration. The photograph clearly shows the difference between the top and bottom surface. The top surface is dark due to the presence of SiC (Figure 16 (a)), while the bottom surface looks metallic (Figure 16 (b)), as the predominant composition is W-Ni-Fe. The same difference was observed when the sample was observed in the SEM. The top surface did not have any tungsten grains, and while the bottom surface had distinct tungsten grains. Figure 17 shows SEM micrographs of the sample (NUC-2) that was electrochemically etched for 30 minutes, followed by electrophoretic deposition of micron-sized particles of SiC. The top and bottom edge of the samples have different microstructures, as the top showed the presence of the SiC phase (dark area), while the bottom has only the W-Ni-Fe phase. Figure 18shows the microstructure of the sample (NUC-4), where no electrochemical etching or deposition was performed. Its microstructure is similar to the microstructure observed in the bottom edge of NUC-2.

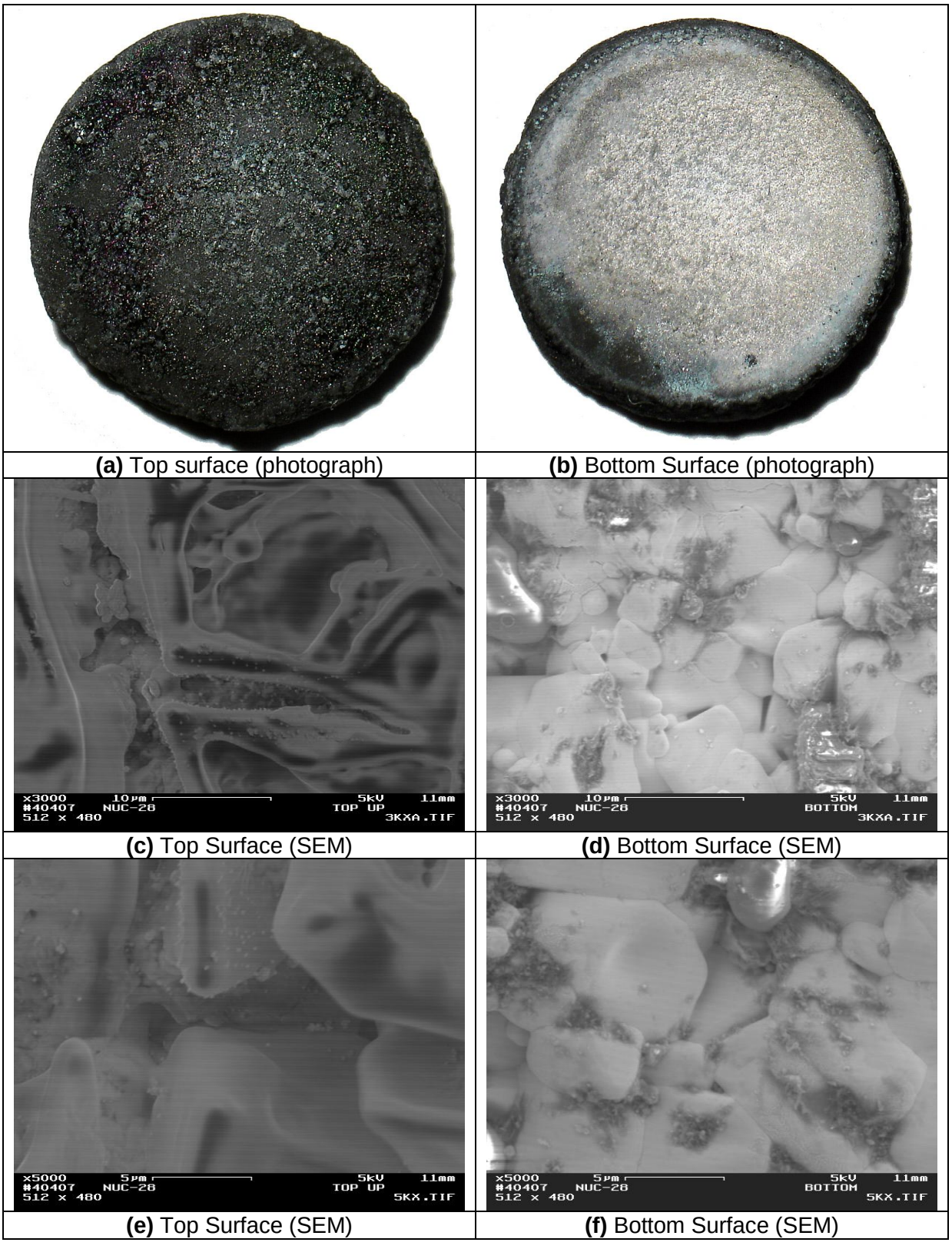

(a) Top surface (photograph) **(b)** Bottom Surface (photograph)

(c) Top Surface (SEM) **(d)** Bottom Surface (SEM)

(e) Top Surface (SEM) **(f)** Bottom Surface (SEM)

Figure 16: Photographs and SEM of NUC-28 after final sintering.

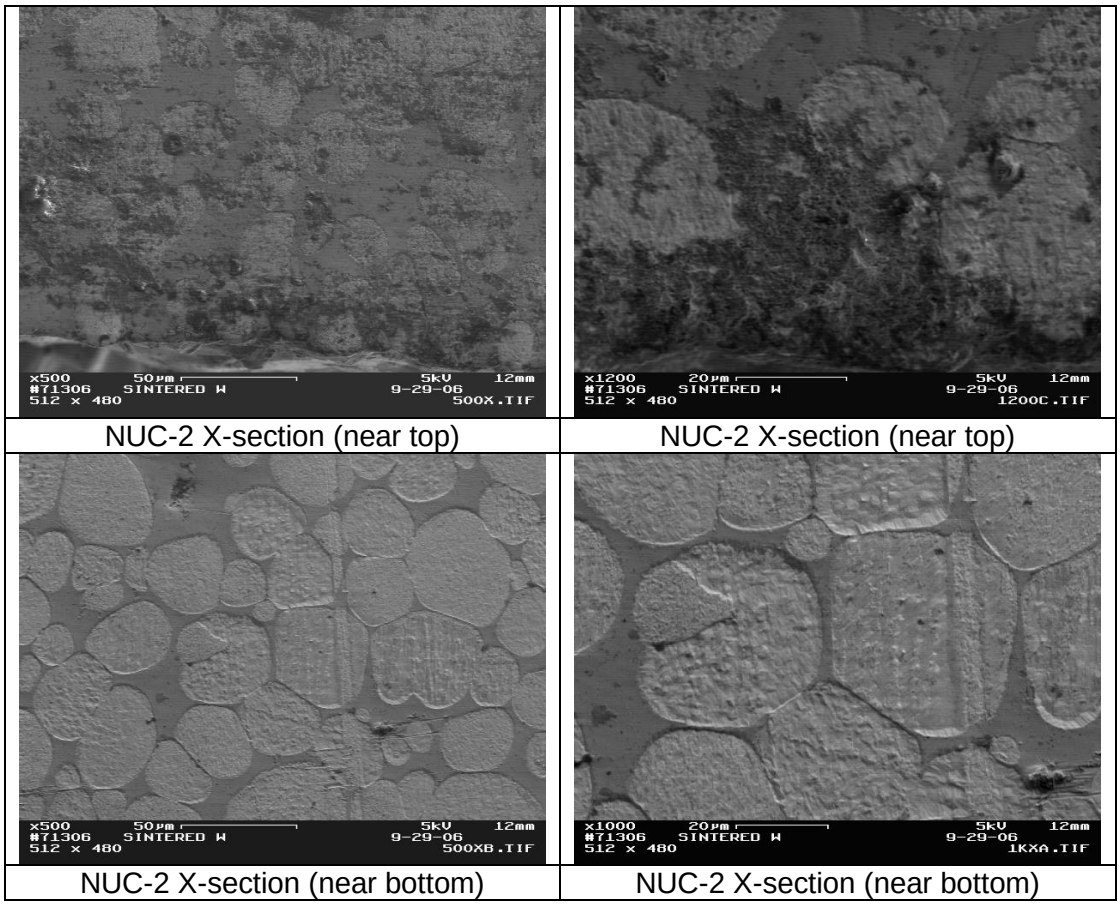

NUC-2 X-section (near top)	NUC-2 X-section (near top)
NUC-2 X-section (near bottom)	NUC-2 X-section (near bottom)

Figure 17: SEM micrograph of NUC-2, after final sintering.

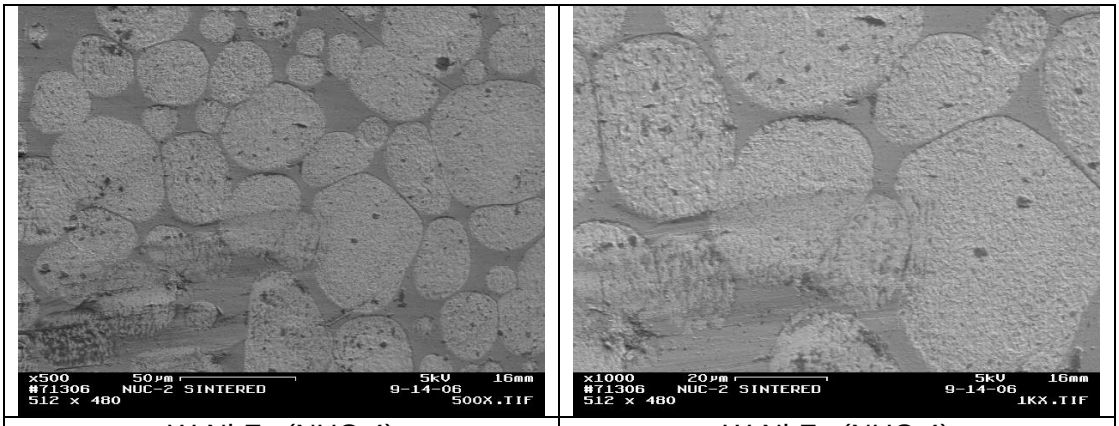

W-Ni-Fe (NUC-4)	W-Ni-Fe (NUC-4)

Figure 18: SEM micrograph of NUC-4 after final sintering.

Figure 19 shows SEM micrographs (cross-section and near the top edge) of the sample (NUC-10) after final sintering. The sample was electrochemically etched, which was followed by electrophoretic deposition of nano-SiC, and infiltration of Ceraset 20. The cross-section, near the top edge, clearly shows the presence of crystalline faceted grains of SiC. The distribution of

the grains shows that they are in the same region where inter-connected pores were present (Figure 19 (c), and (e)), confirming that nano-SiC has indeed infiltrated the pores. The microstructure near the top edge (Figure 19 (b), (d), and (f)), shows the presence of nanocrystalline grains of SiC, which were formed by the decomposition of the Ceraset polymer.

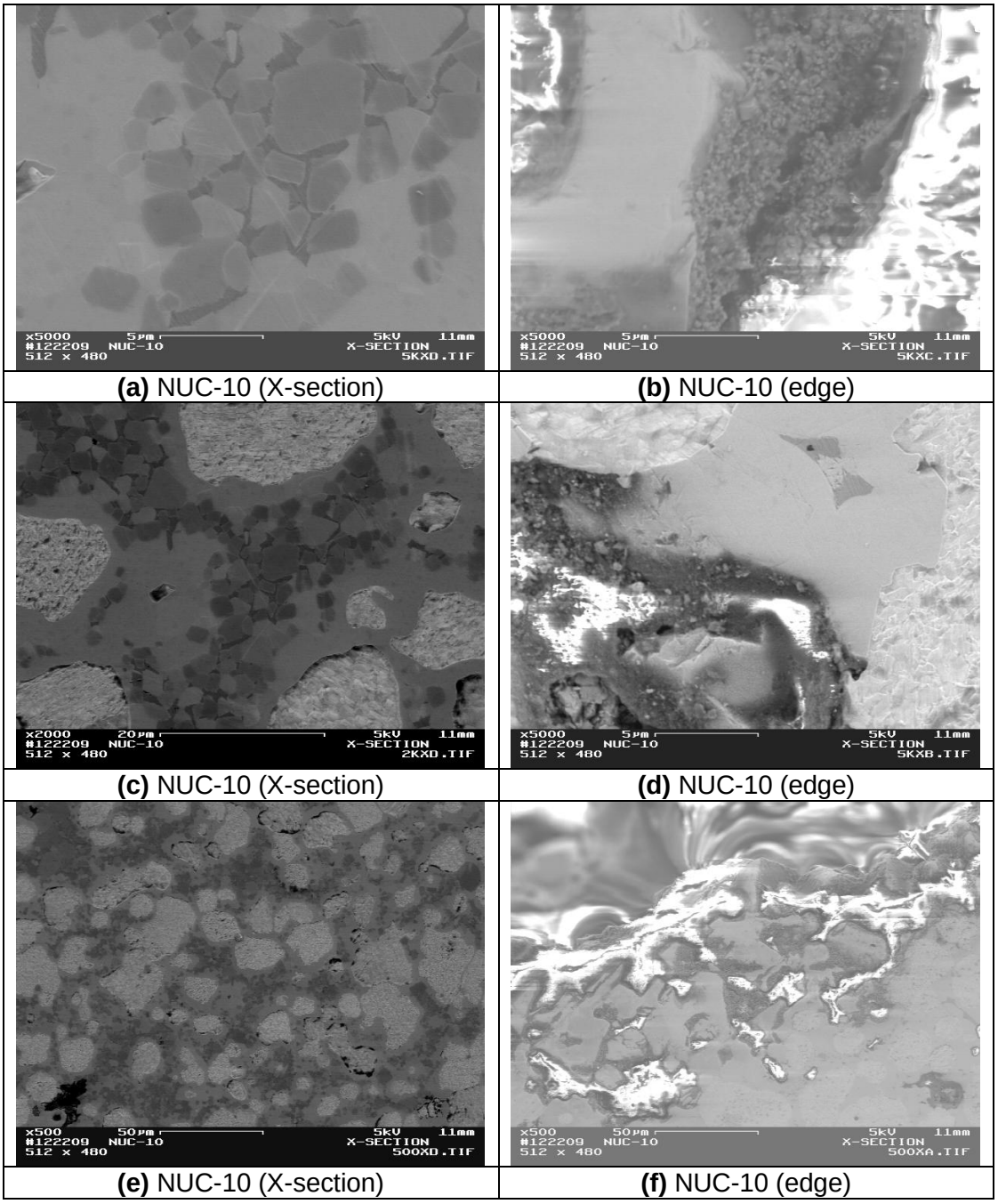

(a) NUC-10 (X-section) | **(b)** NUC-10 (edge)

(c) NUC-10 (X-section) | **(d)** NUC-10 (edge)

(e) NUC-10 (X-section) | **(f)** NUC-10 (edge)

Figure 19: Cross-section and near top edge micrographs of NUC-10, after final sintering.

Table II shows the SiC content of some of the samples, which was determined by the weight gain of the sample, after the final stage of sintering. The maximum amount of SiC, which we were able to infiltrate was 28.2 vol% (corresponds to 6.8 wt%), NUC-24. These samples were

also sent for irradiation testing at MIT Nuclear Laboratory (discussed below). The table also shows the relative content of other elements present in the sample.

Table II: Composition of various samples after final stage sintering

Sample ID	SiC	Ni	Fe	W
NUC-14 & 15	21 vol% (4.6 wt%)	13.6 vol% (8.4 wt%)	2.1vol% (1.15 wt%)	63.7 vol% (85.8 wt%)
NUC-17 & 18	16.4 vol% (3.5 wt%)	14.4 vol% (8.5 wt%)	2.2 vol% (1.16 wt%)	67.1 vol% (86.8 wt%)
NUC-19	0	17.2 vol% (8.8 wt %)	2.6 vol% (1.2 wt%)	80.3 vol% (90 wt%)
NUC-24	28.3 vol% (6.8 wt%)	12.3 vol% (8.2 wt%)	1.9 vol% (1.12 wt%)	57.6 vol% (83.88 wt%)
NUC-25	22.5 vol% (5.1 wt%)	13.3 vol% (8.35 wt%)	2.05 vol % (1.14 wt%)	62.2 vol% (85.4 wt%)
NUC-26	5 vol% (0.98 wt%)	16.3 vol% (8.7 wt%)	2.5 vol% (1.18 wt%)	76.3 vol% (89.12 wt%)
NUC-27	11.2 vol% (2.28 wt%)	15.2 vol% (8.56 wt%)	2.34 vol% (1.17 wt%)	71.4 vol% (87.95 wt%)

D.7 Hardness Measurements

The hardness of the composite (NUC-28) after final sintering was measured using a Knoop indenter. The hardness of the top surface was difficult to measure due to the surface roughness (the sample were not extensively polished, as it would remove the surface SiC). However, based on the approximate measurements, the top surface has a hardness ~3000 Kg/mm^2, while the bottom surface has a hardness ~580 kg/mm^2. These values indicate that the top layer has a significantly higher amount of SiC. The hardness of the W-Ni-Fe sample (NUC-30), sintered under similar conditions was only 240 Kg/mm^2.

D.8 Irradiation Experiments at the MIT Nuclear Reactor Laboratory

The MIT Research Reactor (MITR) is the Nuclear Reactor Laboratory's (NRL) principal experimental facility. The MITR, shown schematically in Figure 20, is a 5 MW tank-type reactor that is fueled with highly enriched uranium-aluminum alloy fuel. The core is light water cooled and moderated, and heavy water/graphite reflected. There are up to four positions available for in-core irradiation facilities. In addition to in-core facilities, several beam ports are available for research and educational uses.

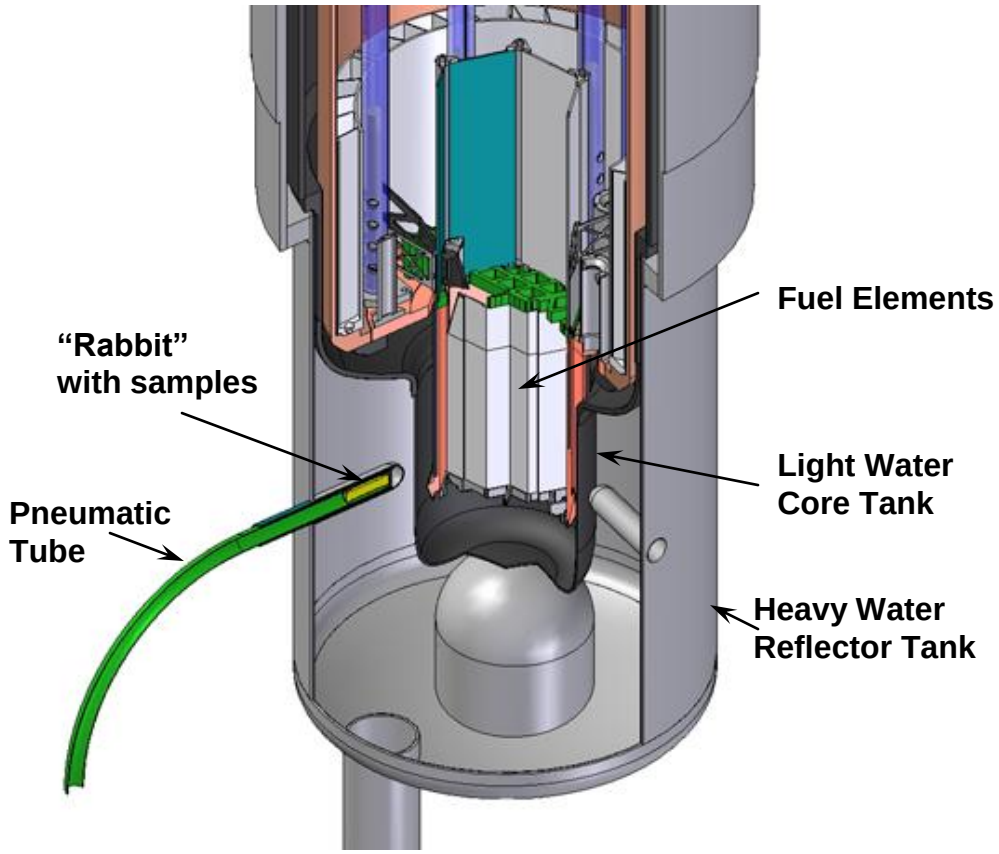

Figure 20: Schematic and/or photograph of the unit where the tests were carried out**.**

For the first test, four functionally graded W-SiC samples were irradiated in a pneumatically-driven 2" beamport that is positioned in the heavy-water reflector core tank. As a result of its positioning, this facility has the highest thermal flux of any of MITR's facilities at 5 x 10^{13} n/cm^2-s when at full power. The facility also has an epithermal flux (defined as energies greater than 0.1 MeV) of 1 x 10^{11} n/cm^2-s. Additionally, the gamma dose measured in this facility is 6.19 MRad/h. The first set of samples was irradiated for two hours in this facility in a polyethylene vessel called a rabbit (Figure 21). The samples irradiated were NUC-14, NUC-17, NUC-24 and NUC-26 which varied in their volume percent of W relative to SiC. No reportable changes occurred following the two hours of irradiation. Photographs of the samples before and after irradiation (Figure 22) were taken with no noticeable distinctions; particularly, no delamination of the SiC layer was noted. Samples were weighed before and after irradiation with no noticeable weight loss. Following irradiation, isotopic analysis was done on a High Purity Germanium detector to detect any unusual or unexpected impurities. None were noted.

Figure 21: Polyethylene vessel (rabbit) used to place the samples in the irradiation chamber.

(a) **(b)**

Figure 22. Pre-irradiation (a) and post-irradiation (b) photographs of sample NUC-14.

For the second test, five W-Ni-Fe - SiC samples were first encapsulated in quartz vials and then irradiated for 96 hours in the same pneumatically-driven beamport. These samples were NUC-15, NUC-18, NUC-19, NUC-25, and NUC-27. Again, these samples vary in their volume percent of W relative to SiC. These samples were irradiated in a titanium vessel because the duration of the irradiation causes polyethylene to become embrittled. The titanium rabbit is pictured in Figure 23. right. Since these samples are highly radioactive (~80 Ci of activity upon ejection), mechanical testing cannot be performed for several months. However, the samples were observed in a hot cell following ejection and no delamination was noted.

Figure 23: Photograph of titanium rabbit used for long duration tests.

We can conclude from these tests that the W-Ni-Fe - SiC materials appear to maintain their stability in gamma and neutron flux fields. However, these are very preliminary tests at low

temperatures and at radiation doses much lower than expected for component lifetimes in reactors. Therefore, more extensive testing is needed. Table III provides information on all the samples fabricated during the Phase I program.

Table III: Description of different types of samples fabricated during the Phase I program

Sample ID	Porosity Gradient Generated	Sides	Type of SiC for electrophoretic deposition	Polymer Infiltration	Irradiation Tested
NUC-1	Yes	1	Micro (~1μm)	No	No
NUC-2	Yes	1	”	No	No
NUC-3	Yes	1	”	No	No
NUC-4	No	0	None	No	No
NUC-5	Yes	1	Micro	No	No
NUC-8	Yes	2			No
NUC-9	Yes	1	None	No	No
NUC-10	Yes	1	Nano	Yes	No
NUC-11	Yes	1	Nano	Yes	No
NUC-12	Yes	1	None	No	No
NUC-13	Yes	1	None	No	No
NUC-14	Yes	2	Nano	Yes	Yes
NUC-15	Yes	2	Nano	Yes	Yes
NUC-17	Yes	2	Nano	Yes	Yes
NUC-18	Yes	2	Nano	Yes	Yes
NUC-19	No	0	None	No	Yes
NUC-24	Yes	2	Nano	Yes	Yes
NUC-25	Yes	2	Nano	Yes	Yes
NUC-26	Yes	2	Nano	Yes	Yes
NUC-27	Yes	2	Nano	Yes	Yes
NUC-28	Yes	1	Nano	Yes	No
NUC-29	Yes	1	Nano	Yes	No
NUC-30	No	0	None	No	No

E. Summary of Phase I Accomplishments

In Phase I, we demonstrated that functionally graded SiC-W composite can be fabricated, with a smooth interface, which can reduce thermal stresses. Specifically, we have

(i) Fabricated fully dense functionally graded SiC – W samples were fabricated;

(ii) Identified glitches in the current processing procedure and laid out plans for improving the process.

(iii) Demonstrated that SiC-W samples fabricated during Phase I can withstand neutron radiation at the levels, which are possible to be tested during short duration of Phase I.